Intra-seasonal relationship between the Northern Hemisphere sea ice variability and the North Atlantic Oscillation

Kentaro Yamamoto,[1,2] Yoshihiro Tachibana,[1,3] Meiji Honda,[4] and Jinro Ukita[5]

Received 13 March 2006; revised 8 June 2006; accepted 9 June 2006; published 29 July 2006.

[1] An intra-seasonal relationship, including a possible feedback, is investigated between the North Atlantic Oscillation (NAO) and a hemispheric-scale seesaw-like pattern dominant in sea ice variability over the wintertime Northern Hemisphere, with one polarity in the Bering and Labrador Seas and the other in the Okhotsk and Greenland-Barents Seas. Statistical analysis using observational data suggests that a particular phase of NAO and anomalous atmospheric circulation in the Pacific during early winter contribute toward the development of the midwinter hemispheric sea-ice seesaw. In contrast, the ice seesaw tends to damp the preexisting NAO signal during late winter, indicating a reversal of the phase relation between them. This NAO damping may be triggered by the Pacific sea-ice anomalies. Results from numerical experiments generally support this notion and further suggests a stationary Rossby wave train emanated from the North Pacific as a dynamical mechanism for damping the NAO signal. **Citation:** Yamamoto, K., Y. Tachibana, M. Honda, and J. Ukita (2006), Intra-seasonal relationship between the Northern Hemisphere sea ice variability and the North Atlantic Oscillation, *Geophys. Res. Lett.*, *33*, L14711, doi:10.1029/2006GL026286.

1. Introduction

[2] The North Atlantic Oscillation (NAO) is one of the predominant modes of atmospheric variability of the Northern Hemisphere (NH) on both interannual and intra-seasonal timescales [e.g., *van Loon and Rogers*, 1978; *Hurrell*, 1995]. Evidence indicates that sea-ice variability over the North Atlantic is linked to the NAO [e.g., *Rogers and van Loon*, 1979]. In fact, the NAO influence is seen in the seesaw-like variability between the anomalous sea ice extents of the Labrador and Greenland-Barents Seas, which is embedded in the dominant pattern of the NH sea-ice variability, defined as the first empirical orthogonal functions (EOF) [e.g., *Deser et al.*, 2000; *Partington et al.*, 2003]. Conversely, recent model studies have suggested that sea-ice variability also influences the atmosphere. *Honda et al.* [1999] pointed out possible downstream influences of the sea-ice variability of the Sea of Okhotsk on the atmosphere over the North Pacific and North America through the formation of a stationary Rossby wavetrain. Further, *Alexander et al.* [2004], *Magnusdottir et al.* [2004], and *Kvamstø et al.* [2004] have suggested through their numerical experiments that sea-ice

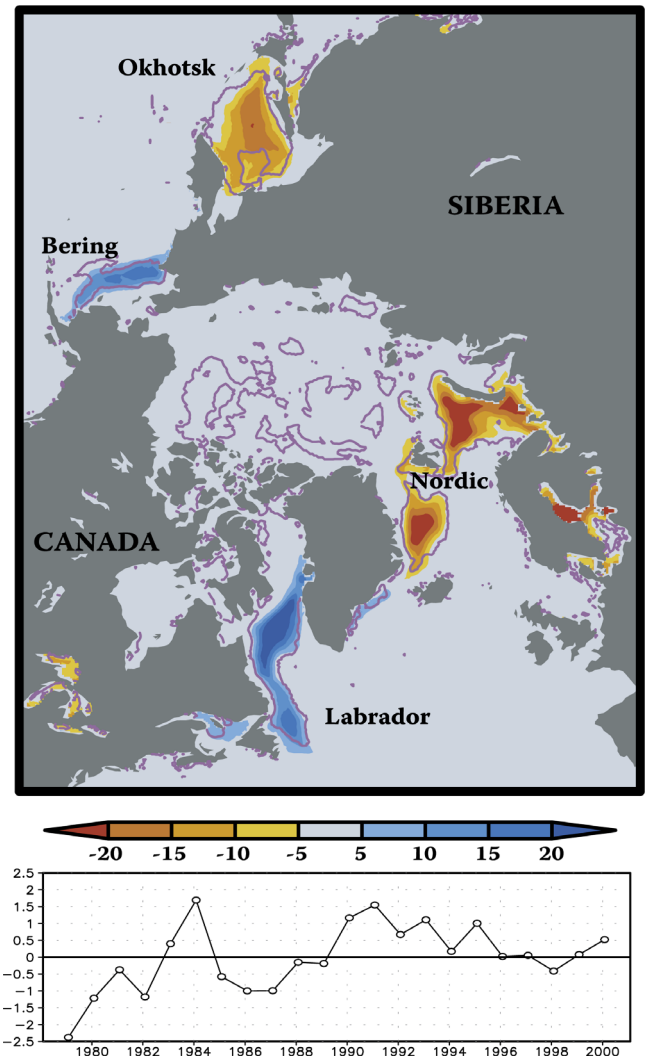

Figure 1. (top) First EOF of February sea-ice concentration (SIC) over the Northern Hemisphere (NH) for 1979−2000. Shadings indicate local anomalies (%) regressed linearly on the corresponding principal component (SIC−PC1) time series (bottom), to represent a local change in ice-concentration when the PC increases by its unit standard deviation. Contours indicate that the correlation between the SIC and SIC−PC1 is significant at the 95% confidence level, based on the *t* statistic.

[1]Department of Aeronautics and Astronautics, Tokai University, Hiratsuka, Japan.
[2]Also at Tokyo Aviation Weather Service Center, Japan Meteorological Agency, Tokyo, Japan.
[3]Also at Institute of Observational Research for Global Change, Japan Agency for Marine-Earth Science and Technology, Yokosuka, Japan.
[4]Frontier Research Center for Global Change, Japan Agency for Marine-Earth Science and Technology, Yokohama, Japan.
[5]Center for Environmental Remote Sensing, Chiba University, Chiba, Japan.

0094-8276/06/2006GL026286$05.00

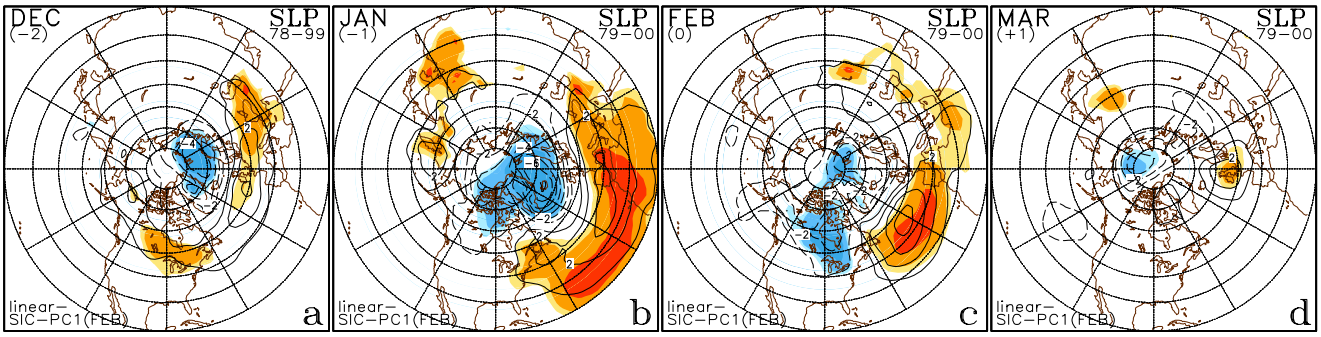

Figure 2. Maps of monthly-mean sea-level pressure (SLP) for (a) preceding December, (b) January, (c) February, and (d) March regressed linearly on the February SIC−PC1 for 1979−2000. Contours correspond to SLP changes (hPa) when the PC increases by its unit standard deviation. Areas of light, moderate, and heavy color shading indicate that the correlation between the SLP and SIC−PC1 is significant at the 90%, 95%, and 99% confidence levels, respectively, based on the *t* statistic.

variability in the Atlantic sector may exert a negative feedback on NAO, for which the Atlantic storm track plays a key role. The present study addresses an issue of how the relationship between the hemispheric-scale dominant sea-ice mode and the NAO evolves during the course of the winter season through statistical analyses using observational data, and model experiments.

2. Data

[3] The sea-ice concentration data used in this study were measured by passive microwave sensors, the Scanning Multichannel Microwave Radiometer on board the Nimbus−7 satellite and the Special Senser Microwave Imager on board the Defense Meteorological Satellite Program satellite [*Cavalieri et al.*, 1997; *Parkinson et al.*, 1999]. We use the monthly data available on a 448 × 304 horizontal-grid (25 km mesh) for 22 recent winters (1978/79−1999/2000). The spatial coverage of this data set is complete in the sense that it includes the whole area of the ice cover in the Sea of Okhotsk. The atmospheric data used here is a reanalysis data set by the National Centers for Environmental Prediction and National Centers for Atmospheric Research jointly [*Kalnay et al.*, 1996] compiled on a 2.5 × 2.5 regular latitude−longitude grid. The NAO-index used here is the difference in the normalized sea level pressure (SLP) between Ponta Delgada, Azores and Stykkisholmur, Iceland [*Hurrell*, 1995].

3. Observational Relationship Between the NAO and Sea-Ice Variability

[4] The leading mode of the NH sea-ice variability is obtained by an EOF analysis on a covariance matrix of the sea-ice concentration (SIC) anomalies for each of the calendar months. The spatial pattern of the first EOF (EOF1) for February is characterized by a hemispheric-scale seesaw between the American and Eurasian sectors (Figure 1), which is composed of a seesaw between the Labrador Sea (LA) and Nordic Seas (NOR), including the Greenland, Iceland, Norwegian and Barents Seas, and another seesaw between the Bering Sea (BE) and the Sea of Okhotsk (OK). We call the particular phase in Figure 1 the "positive" sea-ice seesaw in the present study. This spatial pattern of EOF1 remains robust from January to March, suggestive of the dominance of the seesaw mode throughout the winter season.

[5] To examine a relationship between the NH ice seesaw and atmospheric conditions, SLP anomalies for individual winter months are regressed linearly on the principal component (PC) time series of EOF1 (SIC−PC1) for February. As shown in Figure 2, a positive NAO-like pattern (a pressure dipole with the cyclonic anomaly center to the north) appears from December to March. SLP anomalies are most pronounced in January (Figure 2b). This lagged influence of the January NAO-like signal on the February sea-ice seesaw is also shown as the strongest monthly correlation during winter months (Figure 3).

[6] To examine the details of the atmospheric lagged influence on the seesaw formation in the actual monthly evolution of sea-ice cover, we first define an NH ice seesaw index, as the sum of the North Atlantic (LA minus NOR) and the North Pacific (BE minus OK). This hemispheric ice seesaw index well corresponds to SIC−PC1 as their correlation for February is as high as 0.91. We then regress the SLP field for January on the tendencies (February minus December) of the ice-seesaw indices for the NH, North Atlantic, and North Pacific, separately (Figures 4a−4c). The much stronger signature over the North Pacific in Figure 4c

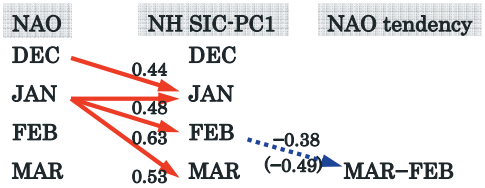

Figure 3. (left) Simultaneous and lag correlation coefficients between the monthly NAO indices and the monthly NH SIC−PC1 for the preceding December to March for 1979−2000. Arrow and the corresponding correlation coefficient are only shown where the coefficient is significant at the 95% (90% for dotted) confidence level. (right) Same as in Figure 3 (left), but for the correlation between NH SIC−PC1 (parenthesis for the North Pacific SIC−PC1) for a particular calendar month and February-to-March NAO tendency.

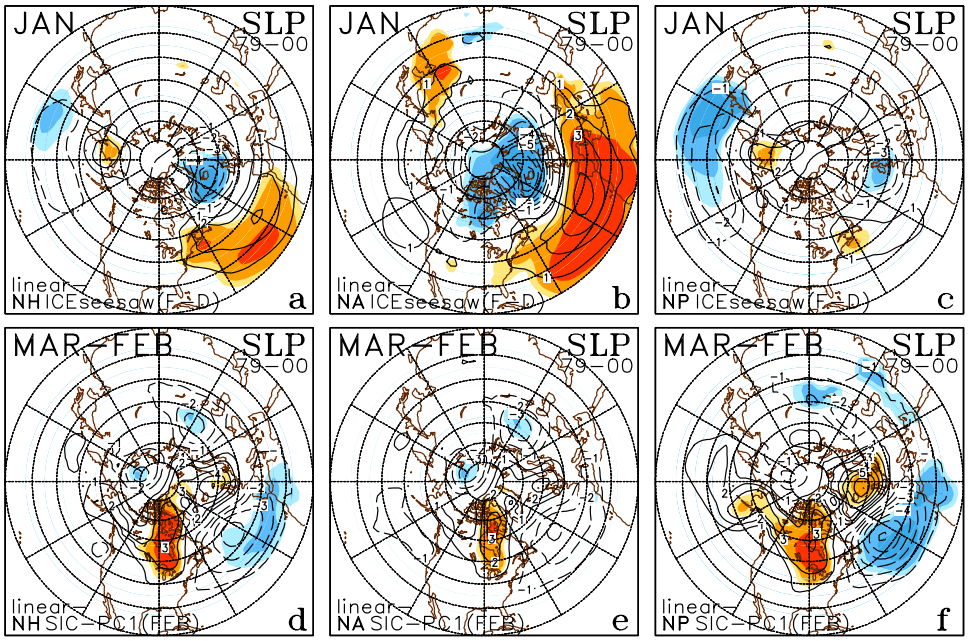

Figure 4. (a–c) Same as in Figure 2b, but for maps of January SLP regressed linearly on the December-to-February tendencies of the ice-seesaw indices for NH (Figure 4a), North Atlantic (Figure 4b), and North Pacific (Figure 4c). Definitions are given in text. (d–f) Same as in Figures 4a–4c, respectively, but for maps of February-to-March SLP tendency regressed linearly on the February SIC–PC1s for NH (Figure 4d), North Atlantic (Figure 4e), and North Pacific (Figure 4f).

than in Figure 4b indicates that the North Pacific ice seesaw is forced locally but not remotely by NAO. Namely, Figures 4a–4c indicate that a particular phase of the NAO and anomalous circulation over the North Pacific in January jointly contribute to form the NH sea-ice seesaw dominant in February. However, the mechanism for the coexistence of the two atmospheric anomaly patterns is still unclear, although the two ice seesaw indices between the North Atlantic and North Pacific are significantly correlated (r = 0.47).

[7] Next, we focus on possible influences of the NH ice seesaw on the atmosphere. A weak signal of NAO with the February SIC–PC1 toward March (Figures 2b–2d) may merely be a manifestation of short persistence of NAO. We prepared two independent 11-year data sets that consist of strong and weak ice-seesaw years based on larger and smaller absolute values of the February SIC–PC1 (Figure 1), separately. The autocorrelations of the NAO index between January and March for the strong and weak ice-seesaw years are 0.09 and 0.53, respectively. Based on the same PC absolute values, it is further confirmed that the difference in the January-to-March NAO tendencies between the six strongest and the six weakest ice-seesaw years is significant at the 95% confidence level based on a *t*-statistic. This difference indicates that the incipient NAO pattern tends to be damped more strongly in the strong ice seesaw years. Noting this difference, the February-to-March SLP tendency field (March minus February) is linearly regressed on the February SIC–PC1s for the NH, North Atlantic and North Pacific, separately (Figures 4d–4f), where these basin-scale PC1s are obtained by an EOF analysis on the SIC anomalies over the Atlantic and Pacific sectors, separately. A negative phase of the NAO is apparently seen in the regression map on NH SIC–PC1 (Figure 4d), suggesting damping the NAO signal. This feature is more clearly seen in the regression map on the North Pacific SIC–PC1 (Figure 4f), which is further confirmed by a strong negative correlation of the February-to-March NAO tendency with North Pacific SIC–PC1 in February (−0.49) than that with NH SIC–PC1 (−0.38) (Figure 3). In comparison, the ice seesaw over the North Atlantic does not significantly damp the NAO signal (Figure 4e). These results suggest that the NAO signal is damped in response to the North Pacific ice anomalies, although other factors may contribute to this.

4. AGCM Experiment

[8] In order to quantitatively examine influences of the hemispheric ice seesaw upon the global atmospheric circulation, we executed an ideal experiment using an atmospheric general circulation model (AGCM). The AGCM used in this study is a global primitive equation model with a spectral transform method, which was developed at the Meteorological Research Institute, Japan [*Chiba et al.*, 1996]. We use a particular version of the model with a triangular truncation at horizontal wavenumber 42 (approximately 2.8° horizontal resolution) and 30 vertical levels. In the model, sea-ice cover is prescribed as a boundary condition and the ice concentration and thickness are assumed to be 100% and 1 m, respectively, where sea ice exists. The climatological-mean sea surface temperature (SST) is prescribed where ice is absent.

[9] A sensitivity experiment of the atmospheric response to the hemispheric sea-ice variability was performed as follows. Based on the observed monthly maximum and minimum sea-ice cover in each of regions, we prepared the positive sea-ice seesaw pattern (maximum in LA and BE and minimum in NOR and OK), as shown in Figure 1, and

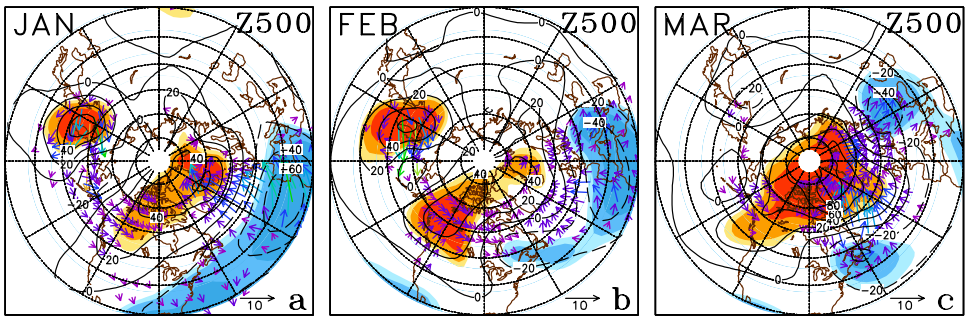

Figure 5. AGCM-simulated differences in 500−hPa geopotential height anomalies (m) for (a) January, (b) February, and (c) March between the ensemble means simulated with the positive and negative ice-seesaw patterns (positive minus negative). Superimposed arrows indicate the horizontal component of a wave-activity flux (m^2s^{-2}, scaled at the bottom) at that level formulated by *Takaya and Nakamura* [2001]. Light, moderate, and heavy color shadings indicate that the differences are significant at the 90%, 95%, and 99% confidence levels, respectively.

the negative pattern with the ice conditions reversed. First we performed a control run for 20 years under the climatological sea-ice and SST conditions. A pair of the 4-month model integrations with the positive and negative sea-ice seesaw patterns was repeated 15 times with different initial atmospheric conditions at the end of November taken from the sixth to 20th model year. We focused on the monthly mean difference field (the positive minus negative patterns) averaged over those 15 pairs of the integrations.

[10] In recognition of equivalent barotropic structure of the atmospheric responses, we here present the model-simulated differences for 500−hPa geopotential height field as the tropospheric response for January, February and March (Figure 5). The most notable difference is an upper-level manifestation of the negative phase of the NAO pattern, which is in good agreement with the observed SLP tendency associated with the hemispheric ice anomaly pattern (Figures 4d−4f). A wave-activity flux [*Takaya and Nakamura*, 2001] as indicated with arrows in Figure 5a suggests that this wavetrain is associated with a stationary Rossby wave emanated around OK [*Honda et al.*, 1999], where the near-surface response is baroclinic and thus favors the upward emanation of wave activity (not shown). The leading edge of the wave train reaches the northeastern part of North America (Figure 5b), and its extension into the Atlantic appears to reinforce the anomalous Icelandic low (Figure 5c).

5. Summary

[11] We investigated evolution of the phase relationship between the NH dominant sea-ice mode and the NAO during the course of the winter season. The positive phase of the NH ice seesaw dominant in midwinter appears as a response to the positive phase of the NAO and anticyclonic circulation anomalies over the North Pacific in early winter. In turn, the midwinter positive sea-ice seesaw damps the incipient positive NAO-like signal. As a result, toward late winter a negative phase of the NAO appears in an atmospheric tendency field. Remote influence from the ice seesaw over the North Pacific is also suggested for the damping of the NAO signal. Our AGCM experiment suggests that in response to the positive NH ice seesaw the negative NAO signal can emerge through a stationary Rossby wave train excited over the OK.

[12] Most of the previous modeling studies emphasized local negative feedback from the Atlantic ice anomalies on the NAO [e.g., *Alexander et al.*, 2004]. Figure 5 suggests that remote influence by a stationary Rossby wave train excited over the North Pacific can effectively enhance the negative feedback over the North Atlantic sector. In another set of the experiments which only OK ice anomalies are imposed, damping of the NAO signal has not been confirmed. With our AGCM experiment alone, one cannot separate the local response to the Atlantic ice anomalies from the remote response from the Pacific. We shall discuss the relative importance between the local feedback and remote influence acting feedbacks, by performing another set of experiments with just the Pacific and/or Atlantic sector sea-ice forcing in the future.

[13] **Acknowledgments.** We thank D. Cavalieri and C. Parkinson for their assistance in providing regional sea-ice data. Our thanks are extended to T. Mikami for technical assistance. Comments by two reviewers were also helpful in revising the paper.

References

Alexander, M. A., U. S. Bhatt, J. E. Walsh, M. S. Timlin, J. S. Miller, and J. D. Scott (2004), The atmospheric response to realistic Arctic sea ice anomalies in an AGCM during winter, *J. Clim.*, *17*, 890–905.

Cavalieri, D. J., P. Gloersen, C. L. Parkinson, J. C. Comiso, and H. J. Zwally (1997), Observed hemispheric asymmetry in global sea ice changes, *Science*, *278*, 1104–1106.

Chiba, M., K. Yamazaki, K. Shibata, and Y. Kuroda (1996), The description of the MRI atmospheric spectral GCM (MRI−GSPM) and its mean statistics based on 10-year integration, *Pap. Meteorol. Geophys.*, *47*, 1–45.

Deser, C., J. E. Walsh, and M. S. Timlin (2000), Arctic sea ice variability in the context of recent atmospheric circulation trends, *J. Clim.*, *13*, 617–633.

Honda, M., K. Yamazaki, H. Nakamura, and K. Takeuchi (1999), Dynamic and thermodynamic characteristics of atmospheric response to anomalous sea-ice extent in the Sea of Okhotsk, *J. Clim.*, *12*, 3347–3358.

Hurrell, J. W. (1995), Decadal trends in the North Atlantic Oscillation: Regional temperature and precipitation, *Science*, *269*, 676–679.

Kalnay, E., et al. (1996), The NCEP/NCAR 40-year reanalysis project, *Bull. Am. Meteorol. Soc.*, *77*, 437–471.

Kvamstø, N. G., P. Skeie, and D. B. Stephenson (2004), Impact of Labrador sea-ice extent on the North Atlantic Oscillation, *Int. J. Climatol.*, *24*, 603–612.

Magnusdottir, G., C. Deser, and R. Saravanan (2004), The effects of North Atlantic SST and sea ice anomalies on the winter circulation in CCM3. part I: Main features and storm track characteristics of the response, *J. Clim.*, *17*, 857–876.

Parkinson, C. L., D. J. Cavalieri, P. Gloersen, H. J. Zwally, and J. C. Comiso (1999), Arctic sea ice extents, areas, and trends, 1978–1996, *J. Geophys. Res.*, *104*, 20,837–20,856.

Partington, K., T. Flynn, D. Lamb, C. Bertoia, and K. Dedrick (2003), Late twentieth century Northern Hemisphere sea-ice record from U.S. National Ice Center ice charts, *J. Geophys. Res.*, *108*(C11), 3343, doi:10.1029/2002JC001623.

Rogers, J. C., and H. van Loon (1979), The seesaw in winter temperatures between Greenland and Northern Europe. part II: Some oceanic and atmospheric effects in middle and high latitudes, *Mon. Weather Rev.*, *107*, 509–519.

Takaya, K., and H. Nakamura (2001), A formulation of a phase-independent wave-activity flux for stationary and migratory quasigeostrophic eddies on a zonally varying basic flow, *J. Atmos. Sci.*, *58*, 608–627.

van Loon, H., and J. C. Rogers (1978), The seesaw in winter temperatures between Greenland and Northern Europe. part I: General description, *Mon. Weather Rev.*, *106*, 296–310.

M. Honda, Frontier Research Center for Global Change, Japan Agency for Marine-Earth Science and Technology, Yokohama 236-0001, Japan. (meiji@jamstec.go.jp)

J. Ukita, Center for Environmental Remote Sensing, Chiba University, Chiba 263-8522, Japan. (jukita@faculty.chiba-u.jp)

Y. Tachibana and K. Yamamoto, Department of Aeronautics and Astronautics, Tokai University, Hiratsuka 259-1201, Japan. (tachi@rh.u-tokai.ac.jp; norick@rh.u-tokai.ac.jp)